NONLINEAR GROUND RESPONSE AT LOTUNG LSST SITE

By Ronaldo I. Borja,[1] Heng-Yih Chao,[2] Francisco J. Montáns,[3] and Chao-Hua Lin[4]

ABSTRACT: A fully nonlinear finite-element (FE) model is developed to investigate the impact of hysteretic and viscous material behavior on the downhole motion recorded by an array at a large-scale seismic test site in Lotung, Taiwan, during the earthquake of May 20, 1986. A stick model with the same spatial interpolation accuracy as a three-dimensional FE model is used for vertical wave propagation analysis. The constitutive model is based on a three-dimensional bounding surface plasticity theory with a vanishing elastic region, and accounts for shear stiffness degradation right at the onset of loading. The model is cast in a time-domain nonlinear FE code SPECTRA and is used to analyze the 1986 earthquake data. It is shown that the recorded downhole motion of Lotung was dominated by nonlinear response. Results of the fully nonlinear analysis are compared with the predictions of the program SHAKE so that the performance of the nonlinear model may be assessed relative to that of an equivalent linear model.

INTRODUCTION

Lotung is a seismically active region in northeastern Taiwan, and was the site of two scaled-down nuclear plant containment structures (1/4-scale and 1/12-scale models) constructed by the Electric Power Research Institute (EPRI) in cooperation with Taiwan Power Company, for soil-structure interaction research (Tang et al. 1990). The site contained a SMART-1 array deployed under a U.S. National Science Foundation grant (Bolt et al. 1982), as well as additional surface and downhole free-field instrumentation in a large-scale seismic test (LSST) array. The local geology at the test site has been established from shear wave velocity and field boring tests (Tang et al. 1990). Soil samples from boreholes up to 150 m deep have also been tested in the laboratory (Wu 1989). Test results suggest that the soil at the site could undergo strong nonlinear response even during moderate to strong earthquakes. On May 20, 1986, a strong earthquake, denoted as the LSST7 event, with magnitude 6.5, epicentral distance of 66 km, and focal depth of 15.8 km, shook the test site. Two downhole arrays located approximately 3 m and 49 m from the edge of the 1/4-scale model, herein called DHA and DHB arrays, respectively, recorded the downhole motions at depths of 0, 6, 11, 17, and 47 m. The objective of this present paper is to analyze the free-field downhole motion recorded by the more distant array, DHB, using a fully nonlinear finite-element (FE) model.

Nonlinear ground response analyses are usually done indirectly via equivalent linear methods (Seed and Idriss 1969; Schnabel et al. 1972; Kausel and Roësset 1984). In these methods, approximate linear solutions are obtained iteratively by assuming constant values of soil properties during the earthquake (Idriss and Seed 1968), but these properties are chosen at the beginning of each iteration according to the strain levels predicted from the previous iteration. These methods work best for one-dimensional wave propagation problems, but could be difficult to implement in a three-dimensional setting. Furthermore, nonlinear wave propagation problems are essentially three-dimensional, since all three components of motion are coupled even if all waves propagate in the same direction, which could lead to further difficulties with the equivalent linear methods. The FE model used in the present study is embodied in a FORTRAN code SPECTRA (Borja and Wu 1994), which is based on a fully nonlinear solution algorithm capable of capturing the coupled multidirectional responses of wave motion through an inelastic soil medium. The LSST7 event is characterized by wave motion in which the incidence angle of S-waves is approximately 6° from the vertical (Chang et al. 1990). Thus, the assumption of vertically propagating shear waves is reasonable, and a one-dimensional stick model is used to capture the nonlinear ground response during the LSST7 event.

The constitutive model of the soil used in SPECTRA is based on a full three-dimensional bounding surface plasticity theory with a vanishing elastic region, formulated in terms of total stresses (Borja and Amies 1994; Borja and Wu 1994). This model automatically captures the shear stiffness degradation and hysteretic damping of soils right at the onset of loading. In the context of the FE model, the nonlinear effects brought about by the elastoplastic constitutive response enter directly into the equation of motion through the internal nodal force vector. Viscous damping enters into the equation through the nodal velocity vector via a viscous damping matrix that is assumed to be stiffness-proportional. Since the constitutive model is based on total stresses, it cannot predict the buildup of excess pore pressures due to cyclic loading. On a related note, there have been no measured values of excess pore-water pressure during the LSST7 event since the pore-pressure sensors at the LSST site were installed in late May of 1986, not early enough for this event (Shen et al. 1989). While it is likely that excess pore pressures did build up during the LSST7 event based on observations made from later events (such as the earthquakes of July and November of 1986), no attempt was made in the present work to include the effect of pore pressure buildup in the simulations.

MATHEMATICAL MODEL

The general FE equation of motion takes the form

$$\mathbf{M}\ddot{\mathbf{x}} + \mathbf{F}_{\text{INT}}(\boldsymbol{\sigma}) = \mathbf{F}_{\text{EXT}} \tag{1}$$

where

$$\mathbf{F}_{\text{INT}}(\boldsymbol{\sigma}) = \int_{\Omega} \mathbf{B}^T \boldsymbol{\sigma}\, d\Omega \tag{2}$$

= internal nodal force vector; $\mathbf{M}$ = consistent mass matrix; $\ddot{\mathbf{x}}$ = nodal acceleration vector; $\mathbf{B}$ = strain-displacement transformation matrix; $\boldsymbol{\sigma}$ = Cauchy stress vector; Ω = problem domain; and T = transposition operator.

[1]Assoc. Prof., Dept. of Civ. and Envir. Engrg., Terman Engrg. Ctr., Stanford Univ., Stanford, CA 94305-4020.

[2]Sr. Engr., Marc Analysis Res. Corp., 260 Sheridan Ave., Palo Alto, CA 94306.

[3]Visiting Scholar, Dept. of Civ. and Envir. Engrg., Stanford Univ., Stanford, CA.

[4]Grad. Student, Dept. of Civ. and Envir. Engrg., Stanford Univ., Stanford, CA.

Note. Discussion open until August 1, 1999. To extend the closing date one month, a written request must be filed with the ASCE Manager of Journals. The manuscript for this paper was submitted for review and possible publication on December 27, 1995. This paper is part of the ***Journal of Geotechnical and Geoenvironmental Engineering***, Vol. 125, No. 3, March, 1999. ©ASCE, ISSN 1090-0241/99/0003-0187–0197/ $8.00 + $.50 per page. Paper No. 12329.

Eq. (1) can be integrated in the time domain (t_n, t_{n+1}) using the second-order accurate α-method as (Hilber et al. 1977)

$$\mathbf{M}\mathbf{a}_{n+1} + (1 + \alpha)\mathbf{F}_{\text{INT}}(\boldsymbol{\sigma}_{n+1}) - \alpha\mathbf{F}_{\text{INT}}(\boldsymbol{\sigma}_n) = \mathbf{F}_{\text{EXT}}(t_{n+1+\alpha}) \quad (3)$$

where $\mathbf{a}$ = algorithmic nodal acceleration vector; and α = integration parameter. The algorithmic displacement and velocity vectors are updated from the incremental formulas

$$\mathbf{d}_{n+1} = \mathbf{d}_n + \Delta t\mathbf{v}_n + \frac{\Delta t^2}{2}[(1 - 2\beta)\mathbf{a}_n + 2\beta\mathbf{a}_{n+1}] \quad (4)$$

$$\mathbf{v}_{n+1} = \mathbf{v}_n + \Delta t[(1 - \gamma)\mathbf{a}_n + \gamma\mathbf{a}_{n+1}] \quad (5)$$

where β and γ = Newmark's time-integration parameters.

Eq. (3) can be cast in residual form as

$$\mathbf{r}(\mathbf{a}_{n+1}) = \mathbf{F}_{\text{EXT}}(t_{n+1+\alpha}) - \mathbf{M}\mathbf{a}_{n+1} - (1 + \alpha)\mathbf{F}_{\text{INT}}(\boldsymbol{\sigma}_{n+1}) + \alpha\mathbf{F}_{\text{INT}}(\boldsymbol{\sigma}_n) \quad (6)$$

In the nonlinear regime, (6) can be solved iteratively by Newton's method to determine the acceleration-time history of motion (Borja 1991; Borja et al. 1993, 1994). Eqs. (4) and (5) then define the displacement- and velocity-time history responses of the soil medium, respectively.

FE Model for Vertically Propagating Waves

When a horizontally stratified soil layer rests on a horizontal bedrock and the in-plane dimensions are infinite relative to the soil thickness, body waves emanating from the dynamic excitation of the bedrock will propagate vertically in a one-dimensional fashion. Letting the vertical direction be noted by the z-axis and the horizontal plane be defined by the xy-coordinate system, the constraints imposed by the condition of vertically propagating waves are

$$\varepsilon_{xx} = \varepsilon_{yy} = \gamma_{xy} = 0 \quad (7)$$

where ε_{xx} and ε_{yy} = two horizontal normal strains; and γ_{xy} = engineering shear strain on the xy-plane.

To see how these kinematical constraints are imposed within the context of the conventional FE solution, consider an eight-node brick column model shown in Fig. 1(a). For this model, the displacement interpolations are

$$u_i(t) = \sum_{A=1}^{8} N_A d_{Ai}(t); \quad i = x, y, z \quad (8)$$

where N_A = shape function for local node A; and $d_{Ai}(t)$ = time-varying nodal displacement of local node A in direction i. The corresponding time-varying normal strains are

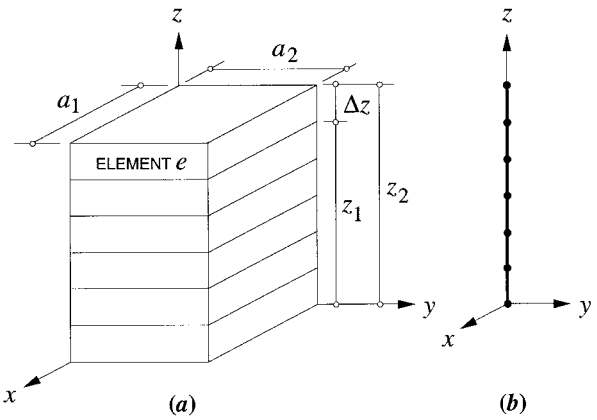

FIG. 1. Modeling Vertically Propagating Waves: (a) FE Mesh of Brick Elements; (b) FE Mesh of Stick Elements

$$\varepsilon_{ii} = u_{i,i} = \sum_{A=1}^{8} N_{A,i} d_{Ai}(t); \quad i = x, y, z \text{ (no sum on } i) \quad (9)$$

while for the engineering shear strains, the corresponding expressions are

$$\gamma_{ij} = u_{i,j} + u_{j,i} = \sum_{A=1}^{8} [N_{A,j} d_{Ai}(t) + N_{A,i} d_{Aj}(t)]; \quad i, j = x, y, z; \; i \neq j \quad (10)$$

Since the nodal displacements cannot be zero, or there will be no motion, the condition imposed by (7) can be satisfied if and only if

$$N_{A,x} = N_{A,y} = 0; \quad A = 1, 2, \ldots, 8 \quad (11)$$

which implies that the gradients of the shape functions with respect to x and y must be identically zero.

Now, the isoparametric interpolations for trilinear brick elements are

$$x = \frac{1}{2}(1 + \xi)a_1; \quad y = \frac{1}{2}(1 + \eta)a_2; \quad z = \frac{1}{2}(1 - \zeta)z_1 + \frac{1}{2}(1 + \zeta)z_2 \quad (12)$$

where (ξ, η, ζ) = respective local element maps of the global coordinates (x, y, z) (Hughes 1987); and (z_1, z_2) = elevations of the bottom and top sides of the element, respectively. Hence, we have

$$N_{A,i} = \sum_{\phi=\xi,\eta,\zeta} N_{A,\phi} \, \text{grad}_i(\phi); \quad i = x, y, z \quad (13)$$

where $\text{grad}_i(\phi)$ = gradient of the local coordinate axis $\phi(=\xi, \eta, \zeta)$ with respect to the global coordinate axis $i(= x, y, z)$, and is obtained from (12) as

$$\text{grad}_i(\phi) = \begin{bmatrix} 2/a_1 & 0 & 0 \\ 0 & 2/a_2 & 0 \\ 0 & 0 & 2/\Delta z \end{bmatrix} \quad (14)$$

where $\Delta z = z_2 - z_1$ = thickness of the soil element. Since $N_{A,\phi}$ is finite for $\phi = \xi, \eta, \zeta$, then the kinematical constraints [(7)] can be satisfied if and only if both $2/a_1$ and $2/a_2$ approach zero. This implies that $a_1 \to \infty$ and $a_2 \to \infty$; i.e., the in-plane dimensions of the brick elements shown in Fig. 1(a) must be infinitely large.

Since both $N_{A,x}$ and $N_{A,y}$ are zero for infinitely large dimensions a_1 and a_2, then N_A must be a function of the element coordinate axis ζ alone. This implies that for a constant z, the resultant displacements of all points in the soil column are the same, and the brick element may thus be replaced by the equivalent line, or stick, element shown in Fig. 1(b). The displacement field for a two-noded stick element consistent with an eight-noded trilinear brick element with infinite in-plane dimensions is given by the FE interpolation equation

$$u_i(t) = \sum_{A=1}^{2} N_A d_{Ai}(t); \quad i = x, y, z \quad (15)$$

Eq. (15) provides nonzero values of the strain components ε_{zz}, γ_{xz}, and γ_{yz}. Similar, though less general, FE modeling was introduced by Prevost (1989) using stick elements that couple only two kinematic components of motion (ε_{zz} and either γ_{xz} or γ_{yz}).

Constitutive Model

Consider a constitutive equation of the form

$$\boldsymbol{\sigma} = \boldsymbol{\sigma}^{\text{inv}} + \boldsymbol{\sigma}^{\text{vis}} = \boldsymbol{\sigma}^{\text{inv}} + \mathbf{D}\dot{\boldsymbol{\varepsilon}} \quad (16)$$

where $\boldsymbol{\sigma}^{inv}$ = inviscid component of $\boldsymbol{\sigma}$; $\boldsymbol{\sigma}^{vis}$ = viscous component; $\dot{\boldsymbol{\varepsilon}}$ = strain rate vector; and $\mathbf{D}$ = material viscous damping matrix. The model described in (16) assumes that $\boldsymbol{\sigma}$ can be decomposed additively into inviscid and viscous parts.

Let us assume that the elements of $\mathbf{D}$ are functions of the frequency level but are independent of the strain level. Hence, in the limit of zero strains, the inviscid components of stresses depend linearly on strains, and so

$$\boldsymbol{\sigma} = \mathbf{C}^e\boldsymbol{\varepsilon} + \mathbf{D}\dot{\boldsymbol{\varepsilon}} \tag{17}$$

where $\mathbf{C}^e$ = elastic stress-strain matrix. Note that $\boldsymbol{\sigma}^{inv}$ typically varies nonlinearly with $\boldsymbol{\varepsilon}$; however the special limiting condition given by (17) is useful for determining the components of the matrix $\mathbf{D}$, since by assuming invariance with respect to the strain level, the components of $\mathbf{D}$ may be evaluated in the limit of zero strains (or elastic response).

Let us now consider the case of isotropic elastic response where $\mathbf{C}^e$ can be expressed in terms of the elastic bulk and shear moduli, K^e and G^e, respectively; and $\mathbf{D}$ can be expressed in terms of the bulk and shear damping coefficients, k and g, respectively. For the case of simple shear, (17) reduces to the following classical Kelvin-Voigt model characterized by linear spring and dashpot arranged in parallel:

$$\tau = G^e\gamma + g\dot{\gamma} \tag{18}$$

For cyclic loading, the hysteretic stress-strain loop generated by this model is defined by the equivalent material damping ratio ξ as (Hardin and Drnevich 1972)

$$\xi = \frac{g\omega}{2G^e} \tag{19}$$

where ω = circular frequency. An equivalent expression may be derived for the bulk damping coefficient k. Thus, for a given damping ratio, the damping coefficients k and g depend on the circular frequency ω.

Of particular interest is the case where $K^e/G^e = k/g$. In this case

$$\mathbf{D} = \frac{2\xi}{\omega}\mathbf{C}^e \tag{20}$$

and so, the material viscous damping matrix $\mathbf{D}$ becomes linearly proportional to the elastic moduli matrix $\mathbf{C}^e$, with the proportionality coefficient being given by the expression $2\xi/\omega$. Since $\mathbf{D}$ is assumed to be independent of the strain level, we can isolate the effect of hysteretic damping induced by plastic deformation and take the value of ξ from the damping ratio curve as the value of the damping ratio in the limit of zero strains. This approach is feasible, since experimental evidence suggests that the damping ratio is really never zero due to energy disspation even at very low strain levels (Kramer 1996).

The next step is to develop the inviscid component of the constitutive model. Here, we consider the three-dimensional J_2-type bounding surface plasticity theory with a vanishing elastic region proposed by Borja and Amies (1994). The model has been enhanced to allow the bounding surface to translate in the stress space (Chao and Borja 1998). Fig. 2 shows a schematic representation of the model, where F and B are two J_2 functions defined such that F always resides in the interior of B. The function F plays the role of the yield function, while B plays the role of the bounding surface; the vanishing of the elastic region then corresponds to the shrinking of F to a point with coordinates $\boldsymbol{\sigma}'$ on the π-plane.

Inside, or on, the bounding surface, we identify the unloading point F_0, with coordinates $\boldsymbol{\sigma}'_0$, such that the hardening modulus H' is infinite at F_0 and approaches a constant value H_0 on the surface B. Fig. 2 depicts the motions of F and B

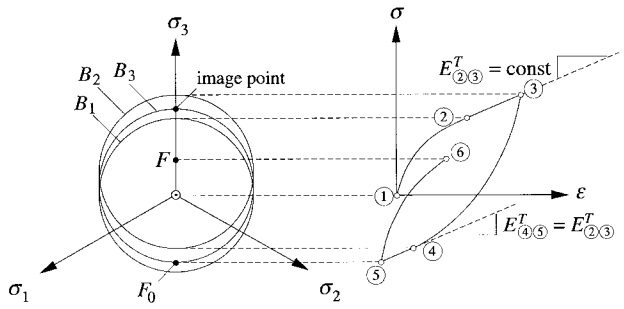

FIG. 2. Schematic Representation Showing Three Positions of Bounding Surface on π-Plane: Soil Is Loaded from Virgin Condition along Path 1-2-3-4-5-6; Final Position of Elastic Nucleus Is *F*

under the case of uniaxial cyclic loading, and shows a final unloading point at the bottom of the final position of B, labeled B_3, where H' is infinite. At the top of the same surface is an image point where $H' = H_0$. The instantaneous value of the hardening modulus H' is then interpolated from the exponential function

$$H' = h\kappa^m + H_0 \tag{21}$$

where h and m = exponential parameters of the model. The dimensionless scalar quantity κ satisfies the condition

$$\|\boldsymbol{\sigma}' + \kappa(\boldsymbol{\sigma}' - \boldsymbol{\sigma}'_0)\| = R \tag{22}$$

where

$$R = \left(\frac{8}{3}\right)^{1/2} s_u \tag{23}$$

= radius of the bounding surface; and s_u = undrained shear strength of the soil [see Borja and Amies (1994) for further details].

For the case $H_0 > 0$, the bounding surface hardens kinematically. Thus, when the elastic nucleus impinges on B, the model reduces to the classical kinematically hardening Von Mises yield theory with associative flow rule in which the bounding surface B now plays the role of the yield function. When the material unloads, as depicted in Fig. 2, the elastic nucleus disengages from the bounding surface but plastic deformation continues to accumulate due to the vanishing elastic region assumption. Consequently, plastic deformation and hysteretic effects are captured naturally by the mathematical model. However, since the model is based on total stresses, it cannot predict the generation of excess pore-water pressure due to cyclic loading.

MODEL PARAMETERS FOR LOTUNG

A seismic survey indicates that the Lanyang plain containing the Lotung array is underlain by two layers of recent alluvium and a Pleistocene stratum resting over a Miocene basement (Anderson and Tang 1989). The local geological profile near the site of the 1/4-scale model shows a layer of gray silty sand and sandy silt about 20 m thick, underlain by about 10 m of gravelly layer resting on a thick deposit of silty clay (Tang 1987). The water table is located approximately at a depth of 1.0 m (Anderson and Tang 1989).

Six material parameters are required by the model to describe the constitutive response of Lotung soil: the (undegraded) elastic shear modulus G^e and Poisson's ratio ν at low strains; the radius R of the bounding surface; the coefficient h and exponent m of the exponential hardening function; and the kinematic hardening parameter H_0 of the bounding surface. In addition, the FE dynamic equation of motion requires values of the total mass density ρ_t and damping ratio ξ. This section

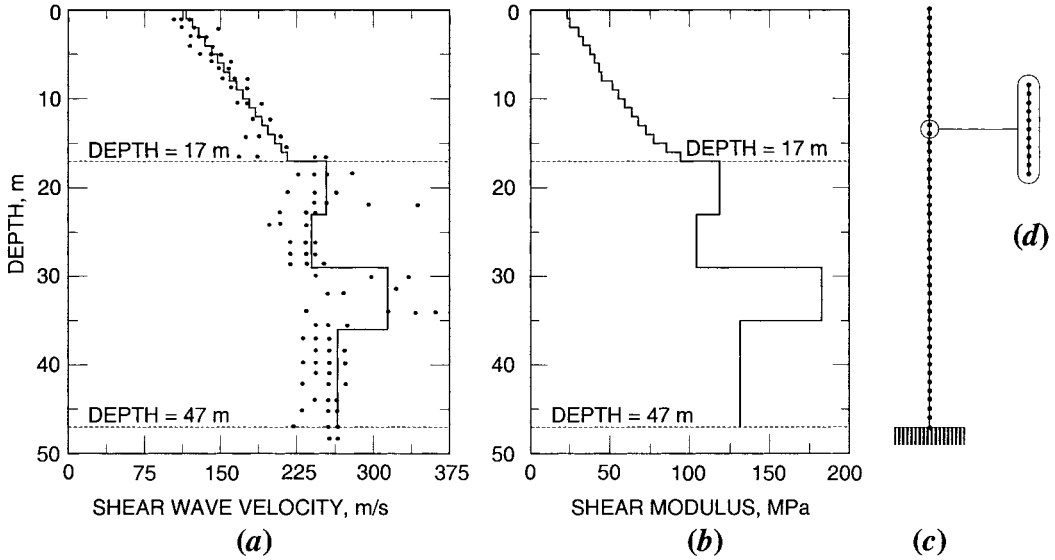

FIG. 3. Local Soil Profile at LSST Site: (a) Shear Wave Velocity; (b) Elastic Shear Modulus; (c) Stick FE Mesh; (d) Refined Mesh for Sensitivity Study

describes the physical significance of these parameters and how their values were determined for the Lotung soil.

The values of G^e were determined from seismic tests. Fig. 3(a) shows the shear wave velocity profile (v_s) obtained from results of seismic crosshole and uphole tests conducted at the 1/4-scale structure location (Anderson and Tang 1989). The shear wave velocity begins at about 100 m/s at the surface and reaches a value of about 300 m/s at 60 m depth. Using measured total unit weights of 19.0 kN/m^3 for the sandy/silty/clayey layer and 19.5 kN/m^3 for the more gravelly layer, an undegraded shear modulus profile was developed from the shear wave velocity profile as shown in Fig. 3(b).

Compression wave velocities (v_p) have also been determined from seismic uphole measurements (Anderson and Tang 1989). Typically, v_p starts at about 300 m/s near the ground surface and increases somewhat linearly to about 1,500 m/s at a depth of 10 m, after which it remains essentially constant. The higher value of v_p is typical of saturated soils (Berger et al. 1989). The values of v_s and v_p at different depths can be combined to estimate the values of Poisson's ratio. Typical values range from a low of 0.46 over the upper 10 m of soil to a high of 0.48 for the remaining soil profile (Berger et al. 1989). Thus, the soil can be considered nearly incompressible. Because the variation of the elastic Poisson's ratio with depth is very small, a constant value of 0.48 has been assumed for the entire soil profile.

A third parameter is the radius R of the bounding surface, which is related to the soil's undrained shear strength s_u through the linear relationship of (23). There is no s_u profile available for the Lotung site, although values of undrained shear strength from unconsolidated undrained tests ranging from 16 kPa to 90 kPa (corresponding to R = 26 and 147 kPa, respectively) have been reported in the literature (Anderson 1993). Theoretically, the value of R can be obtained from the moduli ratio curve as the limit

$$\tau_{max} = \lim_{\gamma \to \infty} \theta G^e \gamma \tag{24}$$

where $\theta = \bar{G}/G^e$ = moduli ratio; $\bar{G}$ = secant shear modulus [assuming the secant shear modulus from the hysteretic curve is equal to the secant shear modulus defined by the backbone curve (Fig. 4)]. The value of R can then be computed as $R = \sqrt{2}\tau_{max}$. The problem lies in determining accurate moduli ratio curves for the soil in question.

Modulus and damping ratio data on soil specimens from

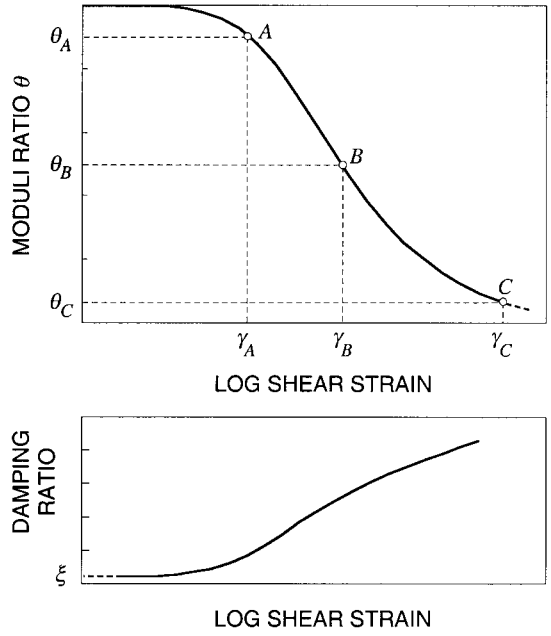

FIG. 4. Determination of Exponential Parameters *h* and *m*, and Viscous Damping Ratio ξ

Lotung have been reported by Anderson and Tang (1989). Unfortunately, these original data had a problem with the conversion of axial strain to shear strain, which was discovered after the EPRI workshop proceedings were published. More recently, Stokoe (Electric 1993) conducted some very careful resonant column and cyclic torsion tests on ''undisturbed'' soil specimens from Lotung. Results of his tests suggest that the modulus ratio data conform fairly well to the upper bound curve proposed by Seed and Idriss (1970) for sand, while the material damping ratio data fall between the mean and lower bounds of the Seed and Idriss curves. However, laboratory experiments are always subject to disturbance effects no matter how carefully they are conducted. An alternative approach, adopted in the present paper, is to back-figure the in-situ moduli ratio curves for Lotung soil based directly on its seismic responses from previous earthquakes, as explained further by Zeghal et al. (1995).

The technique adopted by Zeghal et al. (1995) for back-figuring the in-situ moduli ratio response curves for the Lotung

soil is to integrate twice the recorded acceleration histories at DHB6, DHB11, and DHB17 (from events LSST7, 12, and 16) to obtain the absolute displacements, and then finite-difference the depth to obtain the corresponding shear strain histories. Using a one-dimensional shear beam idealization, the dynamic equation of motion can then be integrated to generate the shear stress histories, from which the shear stress-strain histories can be reconstructed. The accuracy of this approach is a function of the downhole instrument spacing and recorded acceleration wavelengths; for the Lotung test site, the approximation errors are generally less than 2% (Zeghal et al. 1995). For the LSST7 earthquake, Zeghal et al. (1995) developed three curves at DHB6, DHB11, and DHB17. For simplicity in presentation, Fig. 4 only shows one such generic curve.

By choosing a significantly low value of $\theta_C \approx 0.06$, we obtain $\gamma_C \approx 0.01$ from the moduli ratio curves of Zeghal et al. (1995), from which $\tau_{max} \approx 0.0006G^e$ (Fig. 4). Using the elastic shear modulus profile of Fig. 3(b), we obtain values of τ_{max} ranging from a low of 15 kPa to a high of 108 kPa, or values of R ranging from a low of 21 kPa to a high of 152 kPa, in agreement with the values of $R = 26$ kPa and 147 kPa, consistent with undrained shear strengths derived from unconsolidated undrained tests reported by Anderson (1993). Furthermore, the instantaneous tangential shear modulus at this strain level may be used to obtain the plastic hardening modulus for the bounding surface as $H_0 \approx 0.1G^e$. Although data are scarce from the curves of Zeghal et al. (1995) at this high strain level, it must be noted that the Lotung predictions should be relatively insensitive to R and H_0, since analysis results will show that the soil in Lotung did not actually reach this strain level during the LSST7 event.

Borja and Amies (1994) show that the coefficient h and exponent m reflect the overall slope and curvature of the hysteretic stress-strain curve: Higher values of h imply steeper slopes, while higher values of m suggest sharper curvatures of the hysteretic loop. Thus, h and m influence the position and shape of the moduli ratio curve. For the cyclic simple shear stress condition, the steady-state hysteretic curve predicted by the exponential hardening function is given by [compare with (43) of Borja and Amies (1994)]

$$\gamma = \frac{\tau}{G^e} + \frac{3}{2}\int_{-\tau}^{\tau}\left[h\left(\frac{R/\sqrt{2} - \xi}{\xi + \tau}\right)^m + H_0\right]^{-1} d\xi \qquad (25)$$

where $\tau > 0$ is the amplitude of the cyclic shear stress; and $\gamma > 0$ is the amplitude of the cyclic shear strain. In terms of the moduli ratio θ, (25) can be rewritten as

$$1 = \theta + \frac{3}{2\gamma}\int_{0}^{2\theta G^e\gamma}\left[h\left(\frac{R/\sqrt{2} + \theta G^e\gamma - \xi}{\xi}\right)^m + H_0\right]^{-1} d\xi \qquad (26)$$

Eq. (26) can be used to determine h and m, for given values of R, H_0, and G^e. By making this curve pass through two points, say, A and B in Fig. 4, unique values of h and m can be obtained. Here, we choose $\theta_A = 0.9$ for point A and $\theta_B = 0.5$ for point B, yielding $h \approx 1.2G^e$ and $m \approx 0.7$. The choice of these two points, A and B, was initially dictated by the ampleness of data points in the Zeghal et al. curves that fall within the region defined by these two moduli ratio values. Later, it will be shown that the predicted response curves also fall within this range of moduli ratio values so that optimal accuracy is achieved with the use of these two points.

Finally, the material viscous damping matrix **D** was evaluated using (20), together with a value of $\xi \approx 1\%$ obtained from the zero-strain asymptote of the damping ratio curves of Chang et al. (1990) and a value of dominant frequency of $f \approx 0.65$ Hz (or $\omega = 4$ rad/s) obtained from the Fourier transform spectra shown in Fig. 5. In principle, the dominant frequency should be defined from the Fourier transform of the input motion DHB47, since the ground surface response, FA1-5, is actually the result of the analysis, and not the input. This approach gives the expression $\mathbf{D} \approx 0.005\mathbf{C}^e$. The results presented in the next sections show that this viscous damping

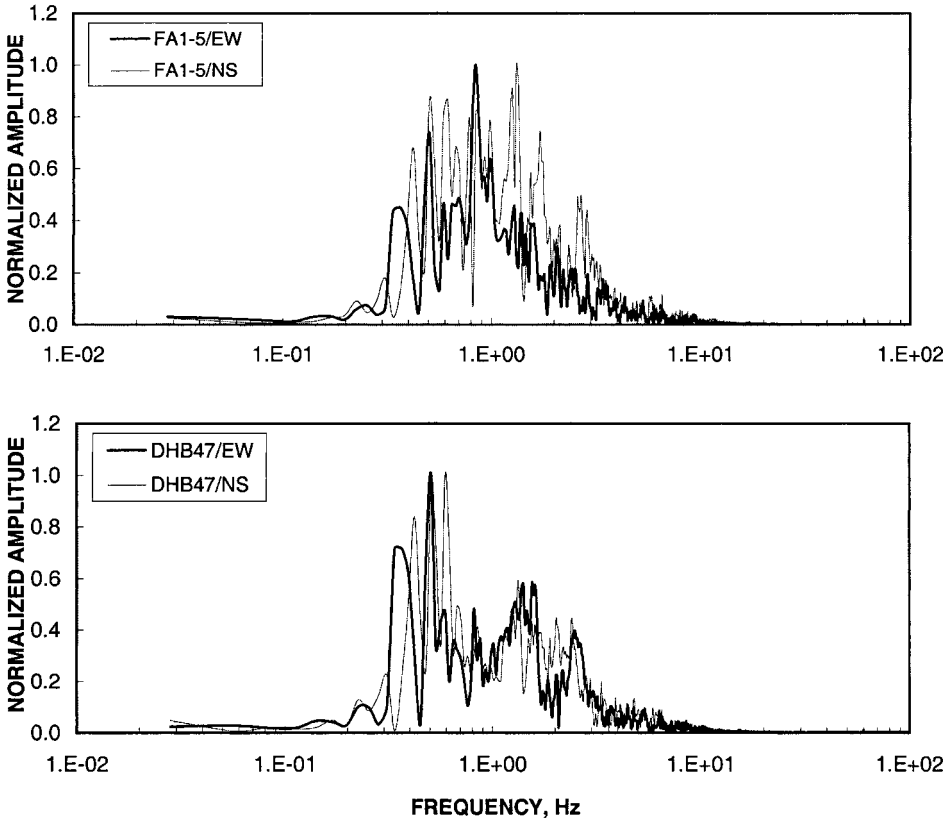

FIG. 5. Fourier Amplitude Spectra of Recorded EW and NS Accelerations

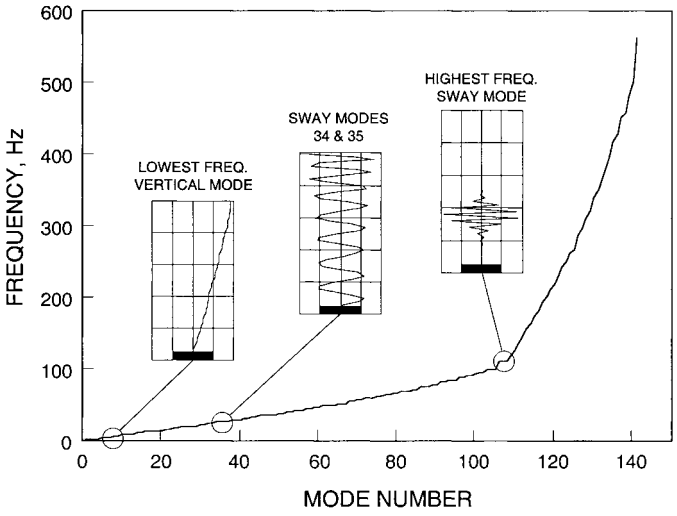

FIG. 6. Vibrational Characteristics of 47-Stick FE Mesh

matrix simply serves to suppress the ''noise'' resulting from the use of the inviscid bounding surface plasticity model, but does not alter the general character of the predicted ground response.

ANALYSIS OF LOTUNG DATA

Fig. 3(c) shows the FE mesh employed in modeling the nonlinear ground response of Lotung assuming the case of vertically propagating seismic waves. The mesh contains a total of 47 stick elements, each having a length of 1 m and defined by two nodes that interpolate the displacement field bilinearly. A standard two-point Gauss rule is used for the numerical integration.

Eigenvalue Analysis

In the limit of elastic response characterized by the undegraded elastic moduli shown in Fig. 3(b), an eigenvalue analysis is possible to study the vibrational characteristics of this FE mesh. Fig. 6 shows the results of such analysis in the form

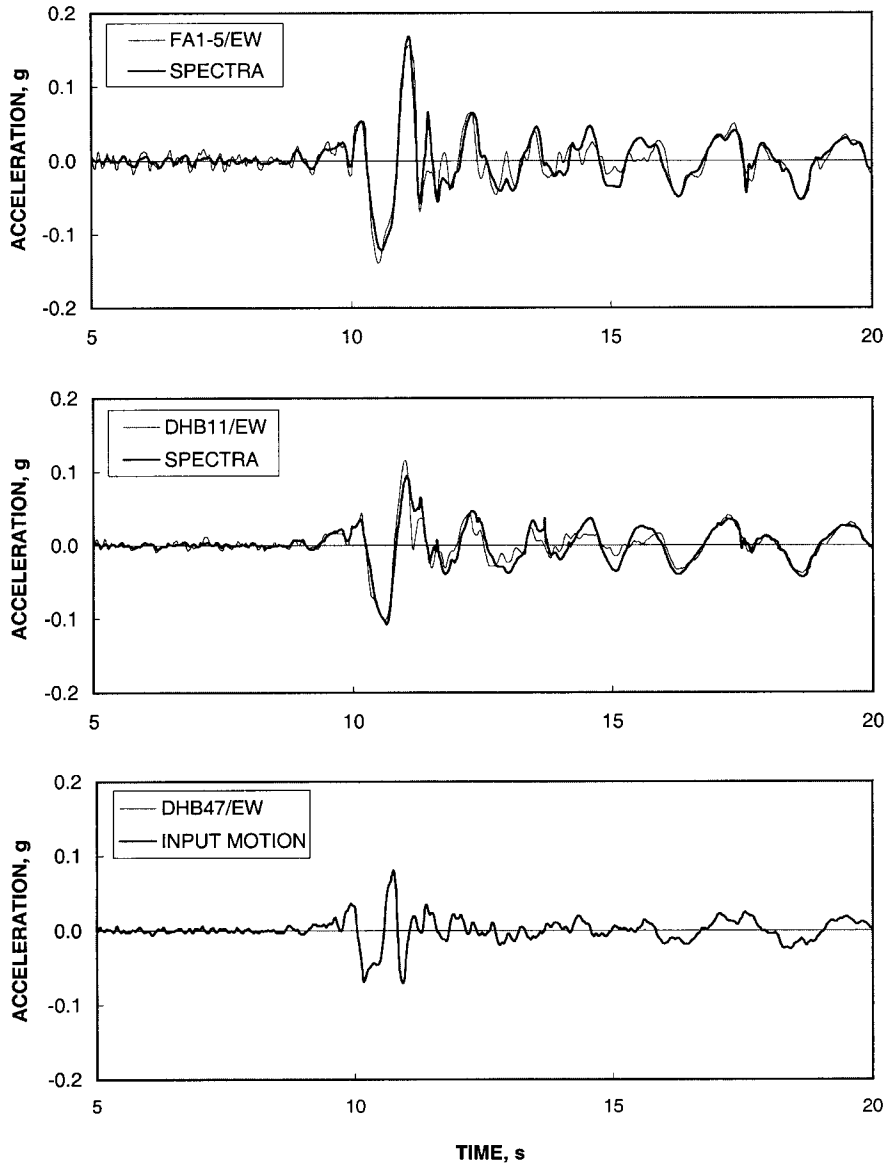

FIG. 7. EW Acceleration versus Time Histories of Downhole Motion for Array DHB

of a plot of natural frequency versus mode number. Assuming that the node at depth 47 m is fixed against translation, the mesh results in a total of 47 × 3 = 141 vibrational modes. The lower vibrational modes are characterized by horizontal sways, while the upper modes are characterized by vertical motion. The horizontal sway modes are repeated in the two perpendicular horizontal directions. The highest frequency horizontal sway mode is around 100 Hz, while that for the vertical mode is around 560 Hz. A comparison with the Fourier transform of the input motion DHB47, shown in Fig. 5, suggests that the 47-stick FE mesh can accommodate most of the frequency contents of the input ground motion. Some typical modes of vibration, including the highest frequency horizontal sway mode, are also shown in Fig. 6.

Nonlinear Analysis

We now simultaneously apply the three components of the input ground motion, east-west (EW), north-south (NS), and up-down (UD), at the bottom of the FE mesh shown in Fig. 3(c), and perform a nonlinear time-domain analysis. Figs. 7–9 compare the downhole acceleration-time histories predicted by the FE code SPECTRA to the motions recorded by the downhole array DHB. The labels FA1-5, DHB11, and DHB47 were used in the original digitized recording and pertain to stations at depths of 0, 11, and 47 m, respectively. The ''bedrock'' was assumed to be at depth 47 m, where the recorded motion was taken as the input excitation. The predictions were obtained using the following values of the time-integration parameters: $\beta = 0.3025$, $\gamma = 0.60$, and $\alpha = -0.10$; the time increment was taken as $\Delta t = 0.02$ s. Borja and Chao (1995) and Chao and Borja (1998) performed additional analyses showing that these values are sufficiently accurate for the Lotung problem. An additional analysis utilizing a refined mesh shown in Fig. 3(d), in which each stick element of Fig. 3(c) was subdivided into 10 elements, was also performed to verify that the 47-element spatial FE discretization is accurate enough for the Lotung problem.

Results of Figs. 7–9 show that peak accelerations are predicted by the nonlinear model to within 10–20% error in all three directions; zero crossings also are predicted quite well. Remarkably, the higher-frequency vertical motions are predicted just as accurately by the model, even though the viscous damping matrix was derived solely from the cyclic shear stress-strain damping ratio. This latter result somewhat validates the assumption that $K^e/G^e = k/g$, leading to a stiffness-proportional viscous damping matrix. A further conclusion points to the following important feature of the nonlinear model: While in principle the three components of motion

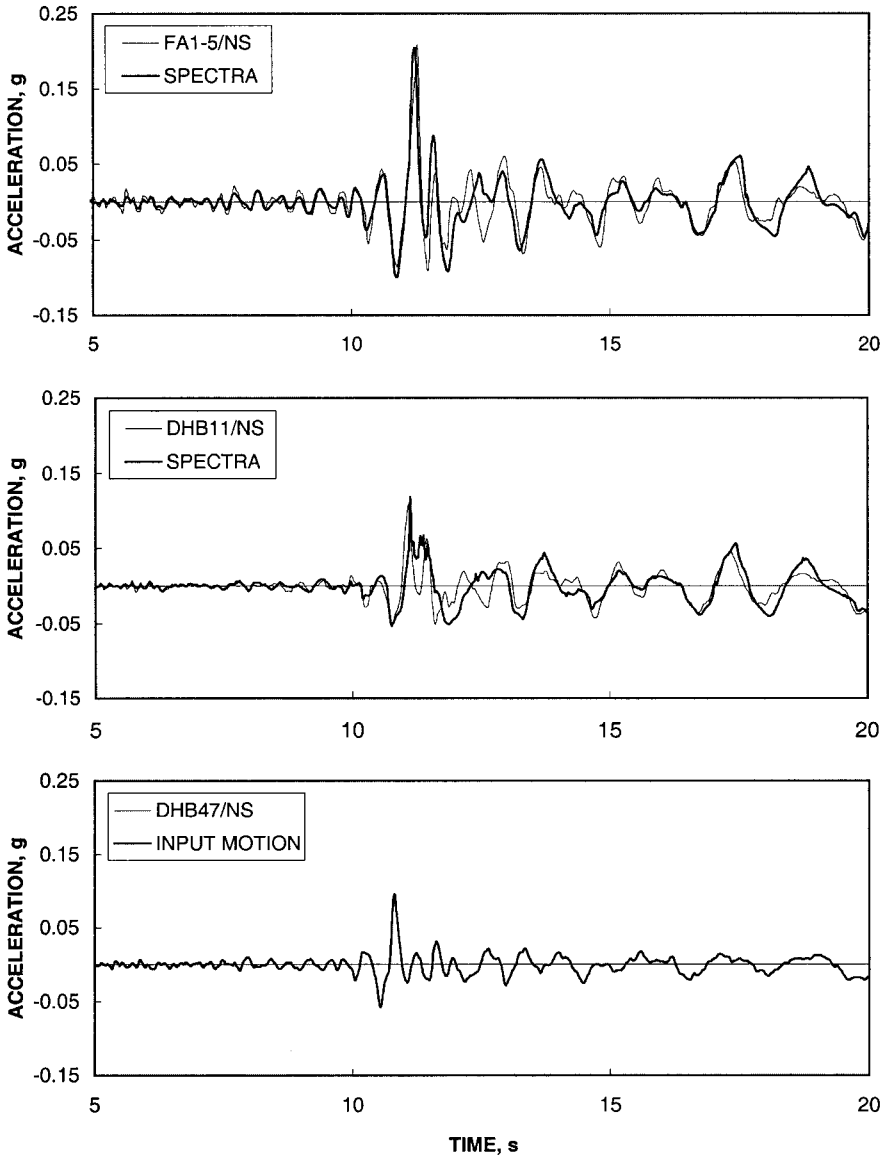

FIG. 8. NS Acceleration versus Time Histories of Downhole Motion for Array DHB

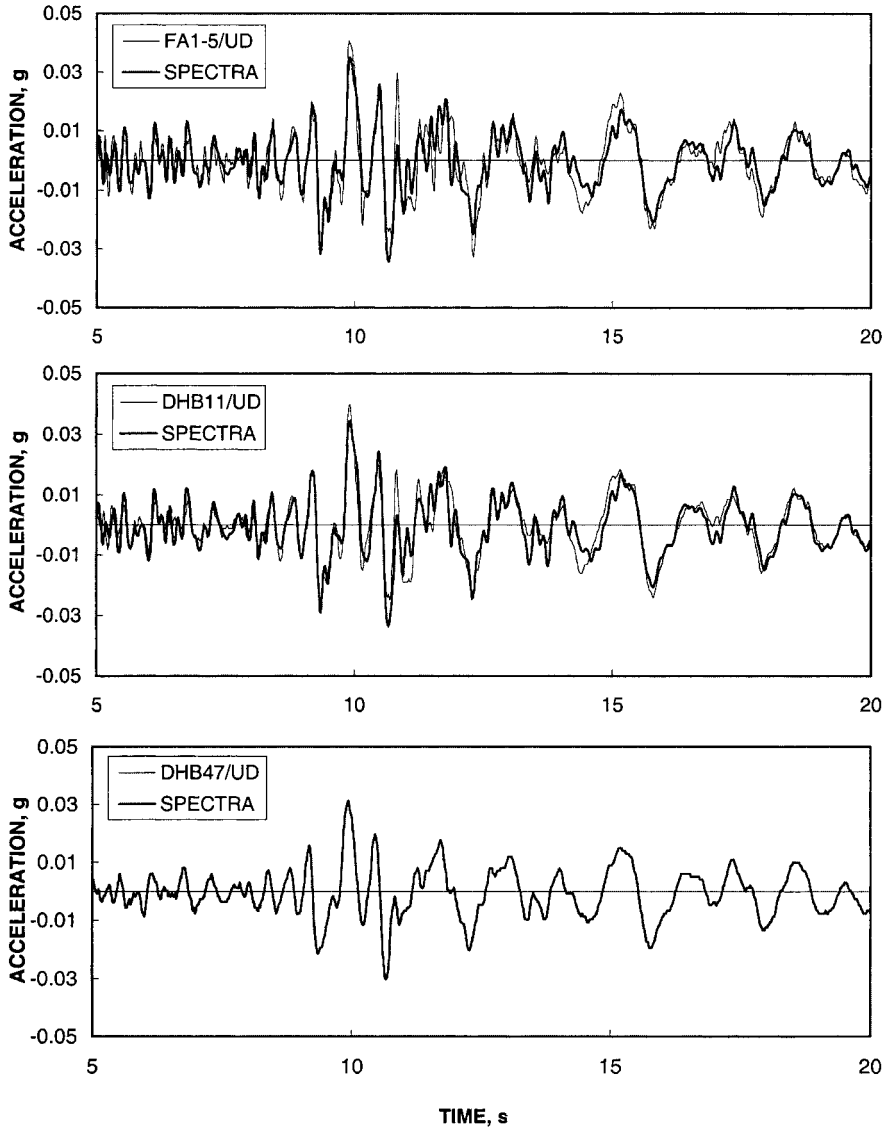

FIG. 9. UD Acceleration versus Time Histories of Downhole Motion for Array DHB

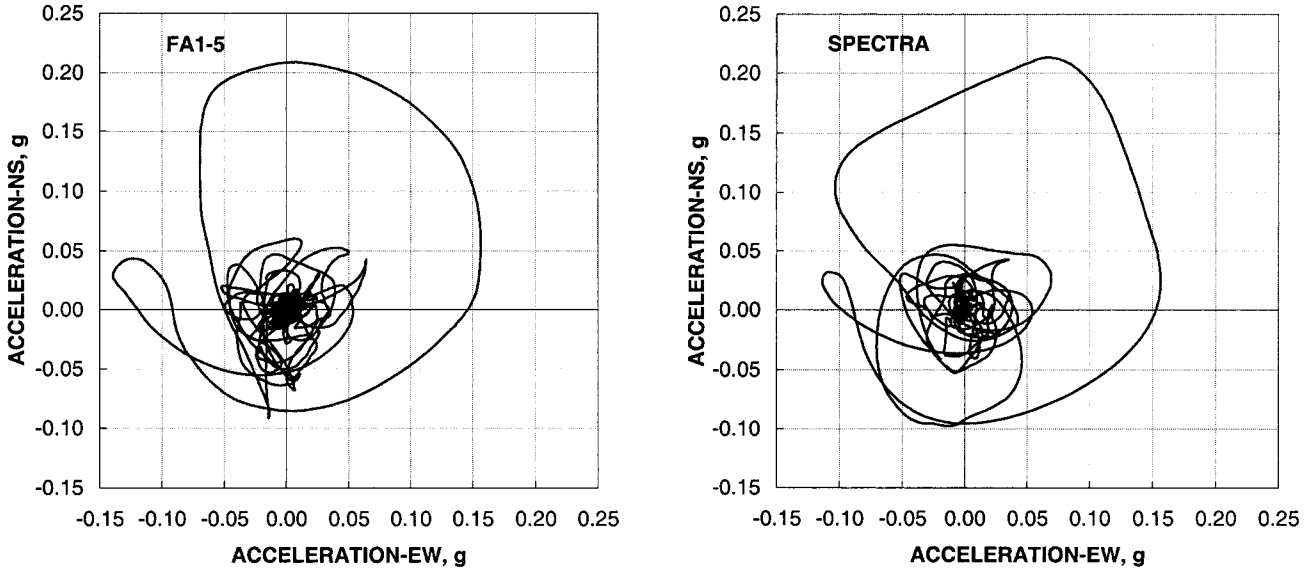

FIG. 10. Comparison of Recorded and Predicted Resolved Ground Surface Accelerations

(EW, NS, and UD) are coupled physically by the plasticity model, only the EW and NS motions produce plastic coupling because of the assumption of vertically propagating waves and because of the deviatoric nature of the bounding surface theory; hence, the vertical motion uncouples from the two horizontal motions, and so energy for the vertical mode is dissipated solely by viscous damping.

To further illustrate the coupled EW and NS motions, Fig. 10 shows a comparison between the resolved horizontal ground surface acceleration recorded by FA1-5 atop the downhole array and the prediction of the numerical code SPECTRA. Note that this comparison is meaningful, since the model fully accounts for the coupled kinematical motions in all three perpendicular directions. While a similar two-dimensional plot can be made from results of equivalent linear analyses such as provided by the widely used computer code SHAKE (Schnabel et al. 1972), such plot would not be as meaningful, since equivalent linear models treat the three components of motion separately. The resolved peak horizontal ground surface acceleration predicted by the nonlinear model compares well with that recorded by FA1-5.

Fig. 11 shows the influence on the EW ground surface motion of (1) suppressing viscous damping by setting $\xi = 0$; and (2) suppressing plastic hysteretic damping by assigning very large values for h and R. The latter simulation is equivalent to forcing the inviscid component of the constitutive model to behave elastically, and so energy is dissipated solely by viscous damping. Clearly, suppressing the viscous damping introduces noise into the solution but does not alter the general character of the predicted ground response. On the other hand, suppressing the hysteretic damping results in a completely uncorrelated ground response, and clearly points to the importance of accounting for plastic deformation to achieve accurate predictions.

It is useful to see how much shear strain is developed in the soil column during the course of the solution. Fig. 12 shows a time history of the maximum resolved shear strain developed over the 47 m depth soil deposit. The maximum

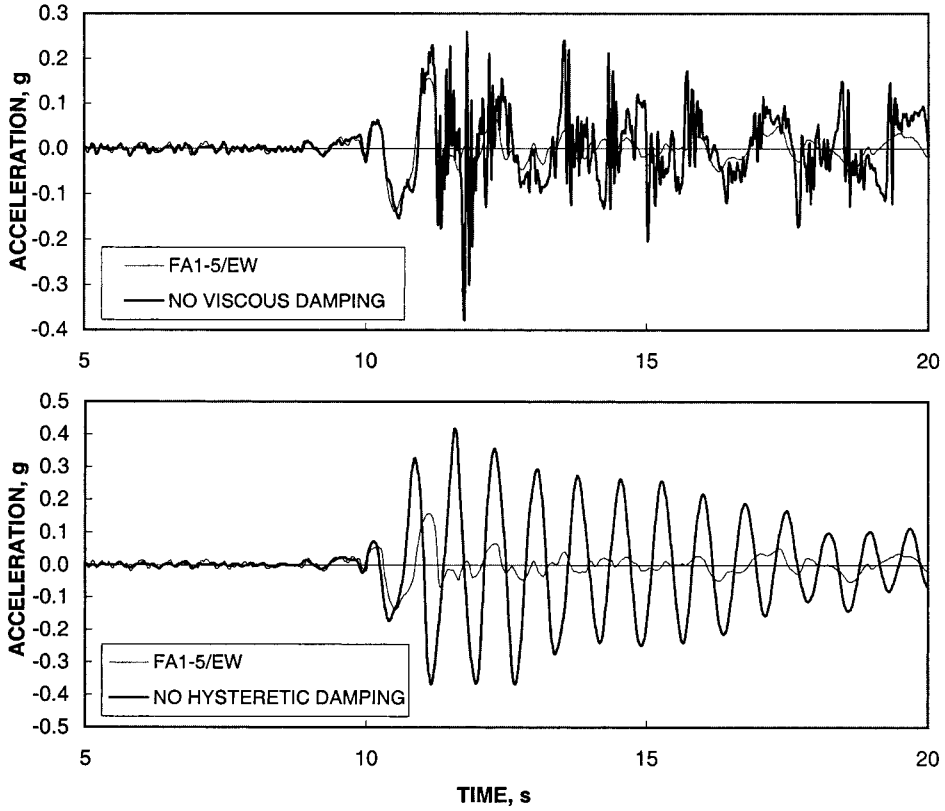

FIG. 11. Isolating Effects of Viscous and Plastic Hysteretic Damping

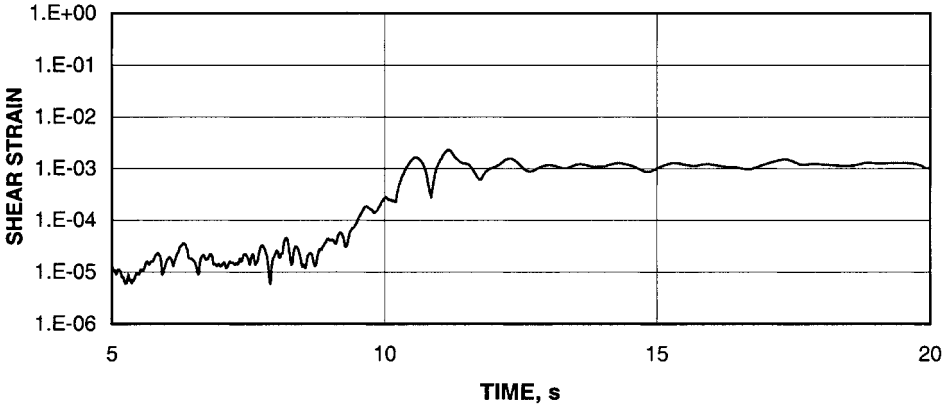

FIG. 12. Time History of Maximum Shear Strain Developed in Soil Column

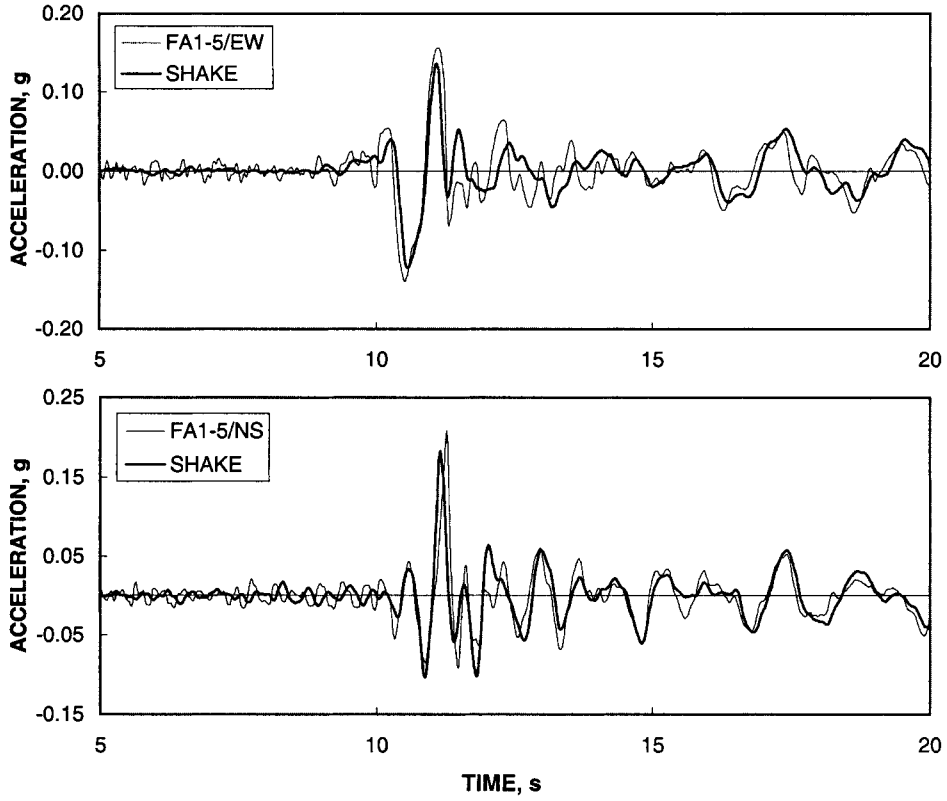

FIG. 13. Comparison of Recorded Ground Surface Accelerations and Predictions by SHAKE

shear strain is calculated by computing, at each time instant, the resolved EW and NS displacement at each nodal point, subtracting the resolved displacements of adjacent nodes to get the relative resolved displacements for each column element, and then dividing them by the element thickness (1 m) to get the resolved shear strain. At each time instant, the column element with the highest shear strain is then identified and the strains are plotted with time. Thus, the maximum strains plotted in Fig. 12 do not pertain to any one specific stick element. The plot of Fig. 12 suggests that the maximum shear strain peaked at around $t \approx 11$ s, which essentially coincides with the arrival of the peak acceleration (Figs. 7 and 8). The maximum shear strain realized throughout the course of the solution is in order of about 0.2%, suggesting that geometric nonlinearity is not even a factor. The maximum shear strain persists beyond this time instant even when the acceleration-time history has essentially died down, suggesting that permanent deformation of this magnitude has developed. Reference to the Zeghal et al. (1995) curves suggests that the shear modulus has degraded to, at most, 20% of its maximum value during the course of the time history. The equivalent damping ratio at this strain level is in the order of 15–20%, well above the assumed viscous damping ratio of 1%, suggesting that energy in the high-strain range is dissipated primarily by hysteretic damping.

Comparison with SHAKE

Using the same moduli and damping ratio curves generated by Zeghal et al. (1995), an equivalent linear analysis of the downhole array data DHB was performed with the program SHAKE (Schnabel et al. 1972). Fig. 13 compares the recorded and predicted ground surface accelerations. Qualitatively, the accuracy of the predictions with SHAKE is just as good, although the peak values were slightly underpredicted. However, note that SHAKE cannot predict the vertical motion unless moduli and damping ratio curves are also available for this mode. In terms of runtime, SPECTRA required about 2.5 min to run all three components of motion simultaneously on a 266-MHz Pentium II personal computer (PC); SHAKE required around 20 s to run one component of motion on the same PC. Note that the runtime for SPECTRA can be reduced further by reducing the resolution of the FE mesh, which is presently well above ''optimal'' for this problem, considering the results of the eigenvalue analysis. The advantage of the nonlinear model lies in its capacity to extend the analysis to three dimensions, and incorporate other important factors such as nonlinear soil-structure interaction and pore-pressure buildup into the analysis.

SUMMARY AND CONCLUSIONS

A fully nonlinear FE model was developed to accurately capture the nonlinear ground response at the LSST site in Lotung, Taiwan, during the seismic event LSST7 of May 20, 1986. The FE formulation is embodied in a FORTRAN code SPECTRA, and accounts for coupled multidirectional components of wave motion through inelastic soil media. The constitutive model is based on bounding surface plasticity with a vanishing elastic region, and incorporates soil stiffness degradation right at the onset of loading. The nonlinear model requires ''standard'' parameters to describe the soil profile: the undegraded elastic moduli, and the moduli ratio and damping ratio curves. In fact, the nonlinear model only requires the zero-strain asymptote of the damping ratio curve to define the viscous component of damping, as the hysteretic part of damping is automatically accounted for by the inviscid component of the constitutive model. Results of the analysis of the LSST7 event show a maximum resolved shear strain of about 0.2% persisting beyond the point of arrival of peak ground acceleration. Most of the energy was dissipated by hysteretic damping, although viscous damping is also essential to suppress the noise associated with the use of an inviscid constitutive model.

ACKNOWLEDGMENTS

Financial support for this research was provided by the Earthquake Hazard Mitigation Division of the National Science Foundation under contract number CMS-9114869, through the program of Dr. C. J. Astill. The writers would like to thank Dr. H. T. Tang and Electric Power Research Institute for making the digitized data for the Lotung site available.

APPENDIX. REFERENCES

Anderson, D. G. (1993). ''Geotechnical synthesis for the Lotung large-scale seismic experiment.'' *EPRI Tech. Rep. No. 102362*, Electric Power Research Institute, Palo Alto, Calif.

Anderson, D. G., and Tang, Y. K. (1989). ''Summary of soil characterization program for the Lotung large-scale seismic experiment.'' *Proc., EPRI/NRC/TPC Workshop on Seismic Soil-Struct. Interaction Anal. Techniques Using Data from Lotung, Taiwan, EPRI NP-6154*, Electric Power Research Institute, Palo Alto, Calif, 1, 4.1–4.20.

Berger, E., Fierz, H., and Kluge, D. (1989). ''Predictive response computations for vibration tests and earthquake of May 20, 1986 using an axisymmetric finite element formulation based on the complex response method and comparison with measurements—A Swiss contribution.'' *Proc., EPRI/NRC/TPC Workshop on Seismic Soil-Struct. Interaction Anal. Techniques Using Data from Lotung, Taiwan, EPRI NP-6154*, Electric Power Research Institute, Palo Alto, Calif, 2, 15.1–15.47.

Bolt, B. A., Tsai, Y. B., Yeh, K., and Hsu, M. K. (1982). ''Earthquake strong motions recorded by a large near-source array of digital seismographs.'' *Earthquake Engrg. & Struct. Dyn.*, 10, 561–573.

Borja, R. I. (1991). ''Composite Newton-PCG and quasi-Newton iterations for nonlinear consolidation.'' *Comp. Methods in Appl. Mech. and Engrg.*, 86, 27–60.

Borja, R. I., and Amies, A. P. (1994). ''Multiaxial cyclic plasticity model for clays.'' *J. Geotech. Engrg.*, ASCE, 120(6), 1051–1070.

Borja, R. I., and Chao, H. Y. (1995). ''Nonlinear ground response analysis at Lotung array test site.'' *Proc., Pacific Conf. on Earthquake Engrg.*, Australian Earthquake Society, Melbourne, Australia, 227–236.

Borja, R. I., and Wu, W. H. (1994). ''Vibration of foundations on incompressible soils with no elastic region.'' *J. Geotech. Engrg.*, ASCE, 120(9), 1570–1592.

Borja, R. I., Wu, W. H., Amies, A. P., and Smith, H. A. (1994). ''Nonlinear lateral, rocking, and torsional vibration of rigid foundations.'' *J. Geotech. Engrg.*, ASCE, 120(3), 491–513.

Borja, R. I., Wu, W. H., and Smith, H. A. (1993). ''Nonlinear response of vertically oscillating rigid foundations.'' *J. Geotech. Engrg.*, ASCE, 119(5), 893–911.

Chang, C. Y., Mok, C. M., Power, M. S., Tang, Y. K., Tang, H. T., and Stepp, J. C. (1990). ''Equivalent linear and nonlinear ground response analyses at Lotung seismic experiment site.'' *Proc., 4th U.S. Nat. Conf. on Earthquake Engrg.*, 1, Earthquake Engineering Research Institute, Oakland, Calif., 327–336.

Chao, H. Y., and Borja, R. I. (1998). ''Nonlinear dynamic soil-structure interaction analysis and application to Lotung problem.'' *J. A. Blume Earthquake Engrg. Ctr. Tech. Rep. 129*, Stanford University, Stanford, Calif.

Electric Power Research Institute. (1993). ''Guidelines for determining design basis ground motions—Vol. 1: Method and guidelines for estimating earthquake ground motion in Eastern North America.'' *Tech. Rep. No. TR-102293*, Electric Power Research Institute, Palo Alto, Calif.

Hardin, B. O., and Drnevich, V. P. (1972). ''Shear modulus and damping in soils: Design equations and curves.'' *J. Soil Mech. and Found. Div.*, ASCE, 98(7), 667–692.

Hilber, H. M., Hughes, T. J. R., and Taylor, R. L. (1977). ''Improved numerical dissipation for time integration algorithms in structural dynamics.'' *Earthquake Engrg. & Struct. Dyn.*, 5, 283–292.

Hughes, T. J. R. (1987). *The finite element method.* Prentice-Hall, Englewood Cliffs, N.J.

Idriss, I. M., and Seed, H. B. (1968). ''Seismic response of horizontal soil layers.'' *J. Soil Mech. and Found. Div.*, ASCE, 94(4), 1003–1031.

Kausel, E., and Roësset, J. M. (1984). ''Soil amplification: Some refinements.'' *Soil Dyn. and Earthquake Engrg.*, 3(3), 116–123.

Kramer, S. L. (1996). *Geotechnical earthquake engineering.* Prentice-Hall, Englewood Cliffs, N.J.

Prevost, J. H. (1989). ''DYNA1D: A computer program for nonlinear site response analysis technical documentation.'' *Tech. Rep. No. NCEER-89-0025*, National Center for Earthquake Engineering Research, State University of New York at Buffalo.

Schnabel, P. B., Lysmer, J., and Seed, H. B. (1972). ''SHAKE—A computer program for equation response analysis of horizontally layered sites.'' *Rep. No. EERC 72-12*, University of California, Berkeley.

Seed, H. B., and Idriss, I. M. (1969). ''Influence of soil conditions on ground motions during earthquakes.'' *J. Soil Mech. and Found. Div.*, ASCE, 95(1), 99–137.

Seed, H. B., and Idriss, I. M. (1970). ''Soil moduli and damping factors for dynamic analyses.'' *Rep. No. EERC 10-10*, University of California, Berkeley.

Shen, C. K., et al. (1989). ''Chapter 25: Pore water pressure response measurements at Lotung site.'' *Proc., EPRI/NRC/TPC Workshop on Seismic Soil-Struct. Interaction Anal. Techniques Using Data from Lotung, Taiwan, Rep. No. EPRI NP-6154*, Electric Power Research Institute, Palo Alto, Calif., 2, 1–20.

Tang, H. T. (1987). ''Large-scale soil-structure interaction.'' *EPRI NP-5513-SR Spec. Rep.*, Electric Power Research Institute, Palo Alto, Calif.

Tang, H. T., Tang, Y. K., and Stepp, J. C. (1990). ''Lotung large-scale seismic experiment and soil-structure interaction method validation.'' *Nuclear Engrg. and Des.*, 123, 197–412.

Wu, W. T., ed. (1989). ''Final testing reports of foundation soils for phase 3 Lotung LSST, Taiwan, Republic of China.'' *Rep. Prepared for Taiwan Power Co.*, National Taiwan University, Taiwan.

Zeghal, M., Elgamal, A. W., Tang, H. T., and Stepp, J. C. (1995). ''Lotung downhole array. II: Evaluation of soil nonlinear properties.'' *J. Geotech. Engrg.*, ASCE, 121(4), 363–378.